Application of Laser-Induced Fluorescence (LIF) to Liquid-Propellant Rocket Engine Testing

C. W. Brasier, J. A. Drakes, and M. A. Simmons
Sverdrup Technology, Inc., AEDC Group
Arnold Engineering Development Center
Arnold Air Force Base, TN 37389-9013

Presented at
AGARD
90th Propulsion & Energetics Panel (PEP)
"Advanced Non-Intrusive Instrumentation for Propulsion Engines"
October 20-24, 1997
Brussels, Belgium

APPLICATION OF LASER-INDUCED FLUORESCENCE (LIF) TO LIQUID-PROPELLANT ROCKET ENGINE TESTING*

C. W. Brasier, J. A. Drakes, and M. A. Simmons
Sverdrup Technology, Inc., AEDC Group
Arnold Engineering Development Center
Arnold Air Force Base, TN 37389-9013

ABSTRACT

Combustion exhausts present a challenging problem for researchers due to the extremely harsh environment, and nonintrusive diagnostics are often sought to provide flow property information. Laser-induced fluorescence (LIF) is one technique in which a chosen flow molecule or marker is probed to yield gross flow properties, such as static temperature and flow velocities. The work presented herein describes the application of LIF to the combustion exhausts of several full-scale liquid-propellant rocket engines spanning a wide range of operational parameters. The method is based upon the use of cw ring-dye lasers which scan in frequency over either the Na D_1 or D_2 line at 5896 and 5890 Å. Na is used as a basis for this approach since it occurs as a trace element in both hydrogen and amine rocket fuels. The generic apparatus is described, including a discussion of the collection and interpretation of the LIF signal to yield radial and temporal profiles of radial flow velocity, static temperature, and fuel distribution. It was found that the LIF technique provides quality data in most cases. Certain stressing situations were also found in which data on the flow properties were not obtainable. Also, computational fluid dyanamics (CFD) modeling of the plumes was used to provide baseline estimates of the exhaust flow properties. The model reasonably predicted the gross behavior of the flow as determined by the LIF technique, although some items of fine spatial structure were not reproduced very well.

INTRODUCTION

The ever-present need to monitor rocket engine health and performance has been a continual driver for the development of nonintrusive diagnostic tools. Much of the work is based upon the premise that information obtained from the exhaust flow at the nozzle exit plane can be directly related to combustion and operational characteristics of the engine itself. The introduction of laser-induced fluorescence (LIF) to the arena of full-scale rocket engine testing has greatly improved the knowledge of exit plane properties. For the past several years, Arnold Engineering Development Center has been modifying the standard LIF techniques to fit the specific requirements of rocket engine testing, at both sea-level stands and simulated high-altitude chambers. To date, three key performance parameters have been determined. These are spatial and temporal resolutions of gas static temperature, radial gas flow velocity, and relative fuel distribution in the exhaust plume flow field. These measurements can be analyzed to provide experimental evaluation of both rocket engine performance and injector mixing/vaporization and overall combustion efficiency.

The key feature of these measurements is that they exploit the inherent sodium impurity present in both amine and hydrogen fuels as a flow probe. The trace amounts of sodium, typically at the parts-per-billion level, are made to fluoresce using a continuous-wave, frequency-scanned dye laser when the excitation source is tuned to 589.0 nm, the absorption frequency of the sodium atom. The fluorescence detection system consists of a set of optically tuned filters and a remote control lensing system placed in front of gain-controlled CCD arrays. The images are recorded at standard video rates on digital tape (D2) recording devices. The images are then digitized using a large-scale video digitizer and placed in a format suitable for computer analysis. Since the sodium atoms serve as a "tag" for the fuel species, radial sodium fluorescence intensity measurements made in the vicinity of the nozzle exit plane can be directly correlated to the radial fuel distribution in the flow. This serves as an indicator of the internal injector mixing efficiency of the oxidizer and fuel streams. The radial velocity of the gaseous exhaust can be determined by the Doppler shift of the sodium absorption frequency. The gas static temperature is provided in a straightforward manner by the Doppler-broadened absorption profile. For altitude testing, the profile is predominantly Gaussian due to the low pressure while at atmospheric pressure, a Voigt spectral line profile is more appropriate. In either case, the temperature is obtained from numerical fitting of the spectral line profile to obtain the line width, and, hence, translational temperature.

The evolution of the LIF technique to full-scale rocket motors can be summarized by reviewing the four measurement programs of Table 1. The engines were the Stennis Space Center Diagnostic Test Facility (DTF) motor, the Space Shuttle Orbital Maneuvering System (OMS), the Space Shuttle Main Engine (SSME), and the Titan IV Second Stage (LR91) engine.[1] The propellants, test conditions, and other details are indicated in Table 1, in which the considerable variation of test parameters and configurations can be seen.

In the following, results from recent measurement efforts at AEDC and several NASA sites will be discussed. Comparisons of the measurement results with the physics-based computational simulations of the exhaust plume flow field properties will be presented. It will be demonstrated that the results obtained from the LIF measurements show good agreement with some of the model predictions, although certain flow features in the data were not predicted *a priori*.

APPARATUS

The essence of the LIF diagnostic method, as developed at AEDC for full-scale rocket engines, is the reliance upon the Na inherently present in the fuels as a result of the fuel manufacturing process.[1,2] For example, the production of the amine

* The research reported herein was performed by the Arnold Engineering Development Center (AEDC), Air Force Materiel Command. Work and analysis for this research were performed by personnel of Sverdrup Technology, Inc., AEDC Group, technical services contractor for AEDC. Further reproduction is authorized to satisfy needs of the U. S. Government. **Approved for public release; distribution unlimited.**

Table 1. Full-Scale Rocket Applicatons of LIF

	NASA Stennis Space Center Diagnostic Test Facility (DTF)	NASA STS Space Shuttle Orbital Maneuvering System (OMS)	NASA STS Space Shuttle Main Engine (SSME)	Titan IV Second Stage (LR91)
Propellants	GH_2/LOX	MMH/N_2O_4	LH_2/LOX	AZ50/N_2O_4
Nominal O/F	5.01	1.6	6.0	1.8
Oxidizer Flow Rate, lbm/sec	1.82	11.8	176.0	211
Fuel Flow Rate, lbm/sec	0.36	7.2	26.1	117
Nominal Thrust, lb	1,200	6,000	500,000	105,000
Nominal Chamber Pressure, psia	484	130	3,200	850
Nozzle Exit Diameter, cm	7.8	110	244	168
Nozzle Cooling Method	Water	Radiation	LH_2 Circulation	Fuel-Film
Area Ratio	6.1	55	77.5	49
Test Location	NASA Stennis	NASA White Sands	NASA Marshall	AEDC
Test Simulated Altitude, km	0	33	0	25
Firing Duration, sec	6 - 27	10 - 168	200	275 - 300

fuel for storable propellant rocket motors utilizes sodium hypochlorite.[2,3] During the combustion of the fuel, the atomic Na is chemically released, making it an ideal tracer to identify the spatial disposition of the fuel in the flow. Furthermore, the optical cross section of Na is very large, requiring only minute quantities of Na to generate measurable LIF signals.[4] Previous applications of the LIF technique demonstrated success with as little as 1 part-per-billion of Na.[5] The LIF measurement technique reported here uses a continuous-wave (cw) laser beam that is propagated across the exhaust flow and frequency tuned in a controlled fashion in a range about the frequency of the Na fluorescence line. The cw laser used in these test programs has a line width of 500 kHz. This implies that the cw laser acts as a very fine probe of the spectral structure of the Na fluorescence line which has a nominal width of 1 to 2 GHz, or 10^3 times the laser width, in this type of application. As the laser tunes, portions of the flow fluoresce to a stronger or lesser extent, depending upon the Doppler-induced frequency shift of the fluorescence line with respect to the laser frequency. Thus, by using a standard video camera operating at a frame rate of 30 frames/sec, it is possible to capture the spatially resolved LIF signal with each video frame corresponding to an average of laser frequencies over the frame integration time interval. For example, if a 30-GHz laser scan requires a 5-sec time interval, the frequency interval averaged in a single video frame is roughly 0.2 GHz. From the video sequence, the spectral shape of the fluorescence line can be reconstructed for each spatial point in the flow. The shape and spectral shift of the spectral line will be used to determine the radial velocity and temperature of the flow.

The basic LIF system is shown schematically in Fig. 1, and the components are described in Table 2. The system consists of an Ar-Ion pump laser, a ring dye laser, a fiber-optic cable to transport the beam into the test cell, a fiber-optic cable head unit located within the test cell, and an absorption detector. The output beam of the pump laser was used to drive a Coherent 699-21 continuous-wave, frequency-scanning ring dye laser. The ring dye lasers have the capability of tuning over a 30-GHz frequency interval centered at either the D_1 resonance line of the Na atom at 5896 Å (corresponding to the transition between the $^2P_{1/2}$ state and the ground $^2S_{1/2}$ state) or the D_2 resonance line of the Na atom at 5890 Angstroms (corresponding to the transition between the $^2P_{3/2}$ state and the ground $^2S_{1/2}$ state). After exiting the dye laser, the laser beam was split by a 60/40 beam splitter into two portions. The weaker portion of the beam was split again, with one beam directed into a Na hollow cathode lamp located on the optics table with the laser, and the other beam directed into a Burleigh WA-2000 wavemeter. The wavemeter measured the gross frequency of the beam, and the Na hollow cathode lamp ensured that the laser frequency was finely tuned to the appropriate Na resonance frequency. The fluorescence generated in the lamp was monitored by a photomultiplier tube, and the output was recorded by a PC-based data acquisition system. Also recorded was the laser scan driving voltage.

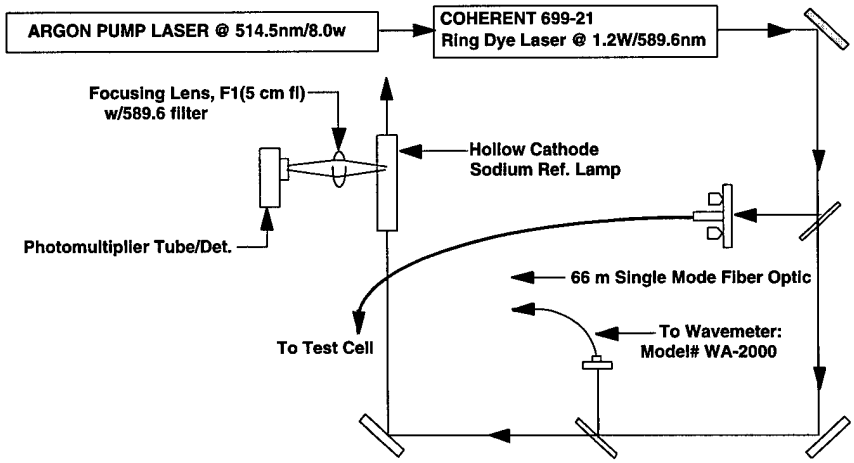

Fig. 1. Na LIF laser system schematic.

Table 2. LIF System Specifications

	OMS
Pump Laser	Spectra Physics 171-09 or Coherent Innova 400-20
Power	8.0 W
Center Wavelength	5145 Å
Dye Laser(s)	Coherent 699-21 scanning ring-dye
Dye	Rhodamine 6G
Linewidth	less than 500 kHz
Power	~1300 mW (out of laser) ~80 mW (out of fiber in test cell)
Frequency Scan Range	30 GHz
Scan Rate	1 scan per 5 seconds
Fiber-Optic Cables	33 or 66 m, 5μm-diam, single mode
LIF Visualization Detectors	1 to 3 gain controlled, CCD camera with 5- or 10-nm Na line filters

The second portion of the ring dye laser beam was directed into a fiber-optic coupler that transferred the beam into a single-mode, 5-μm core, fused silica optical fiber. The terminus of the fiber was in a fiber-optic head unit also containing a beamsplitter and a reference power photodiode detector. The fiber-optic head unit was placed inside the test cell. On the opposite side of the test cell was located a photodiode absorption detector, aligned with the particular laser beam. The voltages from both the reference power and beam absorption photodiodes were also recorded by the PC data acquisition system. A fiber-optic cable was required to remove the laser system from the harsh environment associated with the test cell. The total output of the fibers used was on the order of 100 mW or approximately 25 percent of the incident power on the fiber input coupling lens. A single-mode fiber was implemented to achieve as near a collimated beam as possible, with the resulting output beam diameter being about 3 mm and a beam divergence of approximately 1 mrad. The use of a multimode fiber would result in a much greater beam divergence and, therefore, less collimation would be achieved. It is desired to achieve as near as possible a collimated beam diameter that will closely allow the vertical spatial resolution to match the horizontal spatial resolution. In addition to the reduced laser power available from the fiber, the output polarization changes associated with the fiber birefringence must be considered. The induced birefringence from stresses, movement, or vibration of the fiber greatly impacts the magnitude of laser light reflected off the reference power beamsplitter. This effect must be taken into account when selecting the mounting angle of the reference power beamsplitter, since the reflectivity of the "s" and "p" polarization states has a strong angular dependence.

For the programs presented in this paper, laser operations personnel are required to evacuate the test area approximately 45 minutes prior to motor firing. To ensure proper operation of the laser system during the evacuation period, laser system diagnostics are implemented to remotely monitor laser operations. The diagnostic parameters are not only recorded during evacuation and during motor firing, but also routed to the main control room area where the operations personnel are located during the evacuation period. To reduce the amount of cabling required to transfer these data to the control area, an inexpensive CCD camera is positioned with the laser system to view the metering devices. The resulting video signal is then routed to a video monitor located in the control room so laser personnel can monitor laser frequency, frequency stability, laser power entering and exiting the fiber, the alignment of the beam to the laser absorption detector, and proper operation of the CCD cameras used in the fluorescence detectors inside the test cell.

Once the imagery was collected on the D2 tape format, it was processed using a real-time digitizer at a resolution of 720 pixels horizontally by 496 pixels vertically. The portion of the image in which the laser signal was apparent was summed in the vertical direction, i.e., a spatial integration over the beam profile, at each horizontal pixel, yielding a LIF signal profile for each image. Note that since the laser scan frequency is correlated with the image, every LIF signal profile is associated with a laser frequency. A correction for the angular response of the system, as well as the variation in the laser power as measured by the reference photodiode, was made to each LIF signal profile. In general, background illumination is subtracted from the imagery using a polynomial fit to each video frame in the vicinity of the beam.

To interpret the LIF signal data, a model of the Na fluorescence profile was created, using standard methods. The model was constructed of two pieces, a first-principles model for the spectral shape of the Na fluorescence line, and a downhill simplex or Nelder-Mead algorithm[6] to optimize the free parameters of the spectral line model, i.e., line width, baseline, amplitude, and frequency shift. Although the capability to vary the relative strength of the transitions between the upper ^2P state and the hyperfine components of the lower ^2S state was originally invoked, the ratio of the hyperfine Na line components was eventually set to the nominal theoretical value of 0.375 for the higher energy F_1 line and 0.625 for the lower energy F_2 line.[7] The model used a 1.77-MHz separation between the hyperfine lines. At each of these transitions, a Voigt profile was generated using identical temperatures and broadening parameters. The resulting Na fluorescence line profile was the sum of the two Voigt profiles of the hyperfine components. The entire line profile was then compared to the data. Items not addressed in the Na fluorescence model were pressure shifting of the fluorescence line and radiative transfer of the emitted fluorescence through the plume.

Prior to the tests, the plume flow field was modeled using standard physics-based Joint-Army-Navy-NASA-Air Force (JANNAF) codes, specifically including the flow properties at the axial locations of the LIF measurements. The thrust chamber was modeled using a methodology similar to the Two-Dimensional Kinetic (TDK) computer program[8] for simulating the spatial flow-field properties and performance of axisymmetric thrust chambers. The solution includes the effects of rate-controlled chemical kinetics and approximates a viscous boundary-layer flow near the nozzle wall. Nozzle film cooling and nozzle wall ablation effects were not included in this simulation. The chemical equations and kinetic rates included in the simulation are for the primary combustion reactions involving carbon, hydrogen, oxygen, and nitrogen. Reactions involving trace species such as Na would not significantly influence the overall energy and chemistry and were not included. The thrust chamber solution domain commences in the combustion chamber assuming chemical equilibrium conditions, and subsequently performs a finite-rate chemical kinetics solution through the nozzle throat region and the diverging nozzle region. The solution terminates at the nozzle exit plane, providing static temperature, pressure, radial and axial velocity, and chemical composition, to be subsequently used as initial start-

ing conditions for the plume expansion model. The simulated nozzle exit plane conditions and the free-stream conditions at the simulated test altitude were provided to the Standard Plume Flowfield (SPF) computer program.[9] The near-field plume expansion was simulated from the nozzle exit plane to the test cell diffuser location. The objective of the external plume simulation was specifically to obtain the radial velocity and static temperature profiles at axial positions for comparison with the LIF-deduced profiles.

RESULTS

DTF

The first application of the Na-based LIF by AEDC to full-scale rocket exhausts was at the Stennis Space Center (SSC) on the Diagnostic Test Facility (DTF) thruster engine. The DTF, built for exhaust plume diagnostic sensor development and evaluation, is a 1,200-lbf rocket engine fueled by gaseous hydrogen (GH_2) and liquid oxygen (LOX). The laser system consisted of the same components and layout as described earlier. The laser beam was routed to the test stand from the laser trailer via a 33-m single mode fiber-optic cable delivering a collimated beam approximately 5 mm in diameter and a laser power of approximately 70 mw. System specifications are given in Table 2. System layout relative to the test stand is shown in Fig. 2.

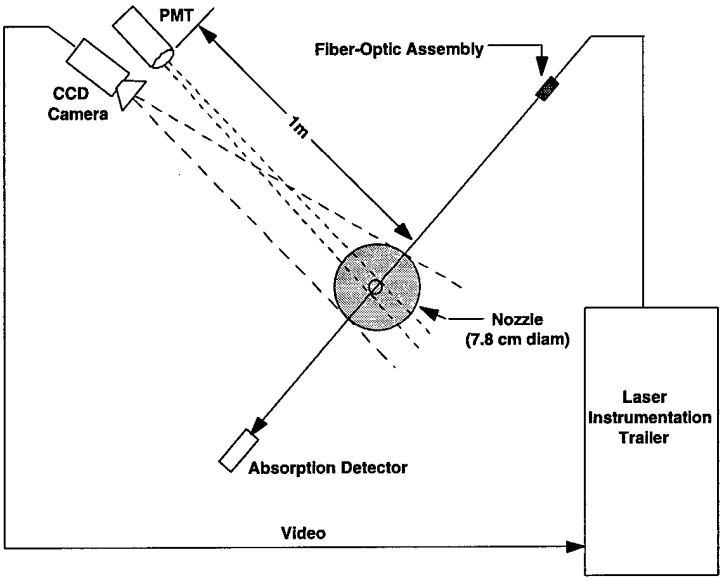

Fig. 2. DTF LIF installation.

Fig. 3. Digitized DTF LIF image.

Video output of the LIF camera and the signal from the absorption photodiode were routed to recorders in the laser trailer. A CCD camera pointed at screens of the primary system diagnostics was used to monitor the status of the controlling electronics. The video was routed to the trailer housing the operating personnel. From this video monitor, operating personnel could monitor proper operation of the equipment prior to engine ignition and during the motor firing. Both video and LIF data were acquired on 14 of 17 firings of the DTF motor. Burn durations ranged from 6 to 27 sec. The O/F ratio for the 14 firings on which LIF data were obtained ranged from 4.65 to 5.41. Sodium concentrations at the nozzle exit plane were estimated to be on the order of 1 ppb.

The data obtained on the DTF plume consist of qualitative flow visualization provided by the sodium-filtered camera. This data set provides information on the positions of the plume boundary and nozzle-induced shock. Figure 3 is a digitized image of a single video frame of the plume taken at the midpoint of the burn. During this test program, it was learned that: (1) Na concentrations of 1 ppb would provide sufficient signal levels for the geometry used on the DTF; (2) system operation using a single mode fiber-optic cable to transfer the beam to the test area is feasible; and (3) a full-field viewing CCD camera can provide point-to-point flow comparisons.

OMS

A program was conducted at the NASA/Johnson White Sands Test Facility (WSTF) to measure radiative and flow-field properties at the exhaust of a Shuttle Orbital Maneuvering System (OMS) engine. This program was sponsored by the Strategic Defense Initiative Organization (SDIO) through the Phillips Laboratory at Edwards Air Force Base, CA. The OMS engine was tested in Test Cell 403 at the WSTF. This cell is a steam-pumped test facility capable of testing engines at simulated altitudes up to 40 km. The OMS engine is a pressure-fed, fixed-thrust, regeneratively cooled system with multiple start and gimbaling capability and uses nitrogen tetroxide (N_2O_4) and monomethylhydrazine (MMH) as propellants. The exhaust nozzle has a 14.8-cm-diam throat and a 109.5-cm-diam exit which provides an expansion ratio of 55:1. The divergent nozzle incorporates a bell contour with an 8.4-deg half-angle and is 146 cm long from throat to exit. The expansion cone is radiation cooled from an area ratio of 6:1 and is fabricated from columbium alloy FS-85. The specific parameters for this test are given in Table 1.

For the OMS test sequence, the cw dye laser tuned across the D_1 absorption line of the sodium atom at 5896 Å. The laser beam was directed across the plume centerline 4 in. downstream of the nozzle exit plane, as shown in Fig. 4. A single gain-controllable, unintensified Dage CCD-72 camera having an array size of 768 pixels horizontally and 493 pixels vertically with a 54-in.-diam field of view, was used as the detector. The camera lens was equipped with a 5-nm bandwidth line filter centered on the D_1 line of the sodium atom. The 30-Hz video output of the camera was recorded on VHS tape using a standard recorder.

Once the initial processing of the imagery was complete, the LIF signal profiles were compiled according to laser frequency scans. For the OMS, approximately 165 LIF signal profiles (5.5 sec times 30 Hz) were acquired during each laser scan. Figure 5 illustrates the set of 165 profiles as a color map in which the 165-pixel vertical dimension is the laser frequency, the 720-pixel horizontal dimension is the radial location across the plume, and the color indicates the value of the LIF signal profile. These data were acquired from 79.3 to 84.8 sec of OMS Test OFL2-6. During this laser scan, the laser tuned from −18 GHz (upper edge) to +12 GHz (lower edge), relative to the Na fluorescence line. The physical extent of the horizontal dimension is from −67.3 to 69.2 cm, relative to the OMS nozzle centerline. Several features of the fluorescence can be clearly observed from Fig. 5, including the vertical slope of the fluorescence due to the Doppler frequency shift. Note the subtle reverses in the velocity apparent in the image, which will be described in more detail below. Also, the large intensity of the Na fluorescence near the outer edge of the flow is apparent, as well as the narrowing of the frequency line width in the most intense region of fluorescence.

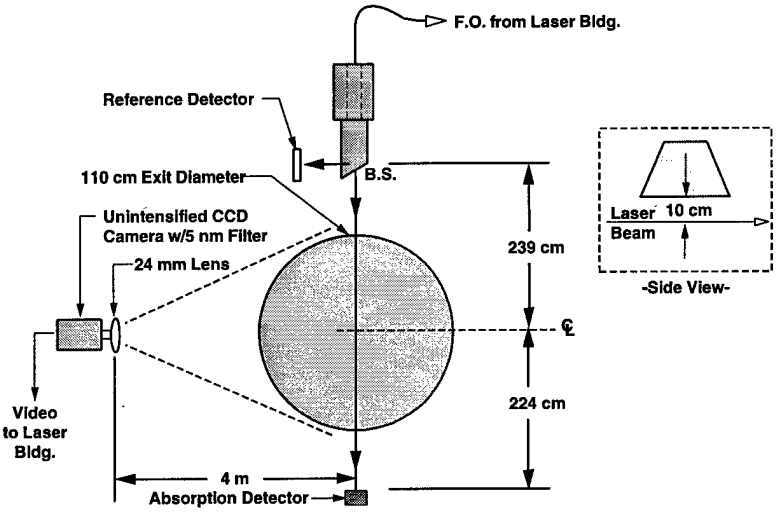

Fig. 4. DMS LIF installation, top view.

Fig. 5. Fluorescence signal acquired during one laser scan from OMS Test OFL2-6.

Figure 6 shows a typical raw LIF image from the OMS test during a time when the laser frequency was near the Na fluorescence line center frequency. The Na fluorescence model was applied to the data, such as that shown in Fig. 5. Figure 7 shows three spectral profiles taken from Fig. 5, at radial positions in the flow of 10.4, 46.5, and 55.9 cm relative to the nozzle centerline. Recall from Table 1 that the nozzle radius is 55 cm; hence, the plume has expanded compared to the nozzle at this axial station. First note that since all three profiles are acquired on the side of the nozzle where the exhaust flow is approaching the laser, the frequency shift is to progressively higher frequencies for positions farther from the nozzle centerline. This is reflected by the radial velocity determined for each spectral profile as denoted on the figure. Also, note the relative heights of the three spectral profiles where it is seen that the outer region of the flow has a much higher density of Na than does the inner portion. In addition, the structure of the fluorescence is clearly evident for the low-temperature region near the center, where it is possible to discern the two hyperfine components. As the temperature increases toward the outer region of the flow, this structure becomes washed out. Finally, note the excellent agreement of the fit to the data.

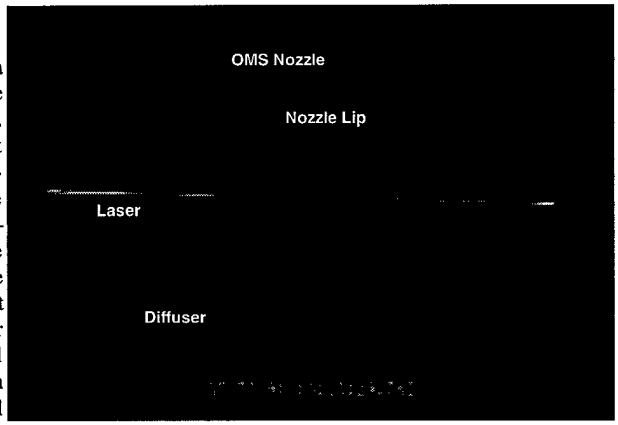

Fig. 6. Raw Image from OMS Firing OFL2-6.

Figure 8 displays the radial velocity observed at three times in the burn, roughly 4, 73, and 120 sec, as a function of radial distance across the plume. It is interesting to note the repeatability of the experimental results at the widely separated times. Also shown on this plot is the result of the SPF calculation. Overall, the agreement of the CFD model with the data is rather good for regions away from the center. Note, however, the feature in the data at ± 35 cm, which is not evident in the model results. In the region from −20 to 20 cm, there exists a signifi-

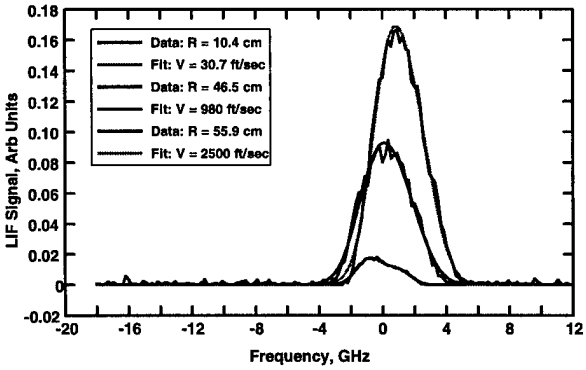

Fig. 7. Spectral profiles and fits taken at three radial positions of Fig. 5.

cant discrepancy between the model and the data. Posttest modeling of the start conditions was able to replicate the measurement results. These discrepancies are much larger than the uncertainty of the data, which is dominated by the systematic term due to the averaging of the laser frequency during individual video image acquisition. Since the camera averages the fluorescence signal for 33 msec while the laser is continuously scanning (at a rate of 30 GHz over 5.5 sec for OMS), the systematic radial velocity uncertainty is $\pm 2.5 \times 10^3$ cm/sec.

The results for the exhaust flow static temperature for this test are shown in Fig. 9, as well as the SPF modeling result. The systematic uncertainty due to the frequency averaging results in a minor uncertainty, nominally ± 50 K for most of the flow. The prediction is in qualitative agreement with the data in the core flow region. Near the flow axis, the prediction is only slightly lower than the data, but the agreement worsens significantly farther from the plume centerline. The plume core is seen to be extremely steady as a function of time, as indicated by the three temperature profiles taken at different times of the burn. There is a qualitative disagreement of the data with the model near the shear layer interface. The data show two peaks in the temperature near the outer flow edges, at roughly ± 52 and 58 cm. (Note the peak at –60 cm in Fig. 9 is an artifact.) The SPF model shows a smeared peak located between the two data peaks, perhaps indicating the limitation of the shear layer mixing model. Even more interesting is the temperature variation of the shear layer peaks as a function of time. Clearly, the inner core flow temperature is steady during the entire burn. However, the shear layer temperature peaks exhibit a curious variation in time in which the outer peak temperature rises during the burn while the inner peak decreases. One possibility for this is the convective heating of the external free stream during the burn, causing the outer peak temperature to rise. Simultaneous with the radiative heating is the cooling of the boundary-layer flow adjacent to the nozzle interior, which would serve to decrease the temperature of the inner peak. Further analysis is required to verify this hypothesis, but it is noteworthy that the LIF data can track small changes in the flow character during the firing.

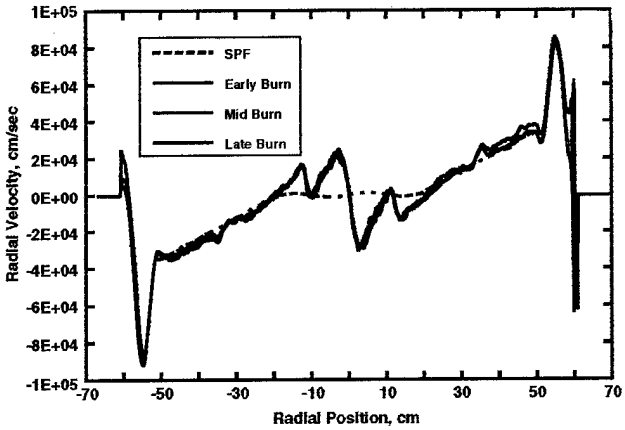

Fig. 8. Measured radial velocities of OMS Test.

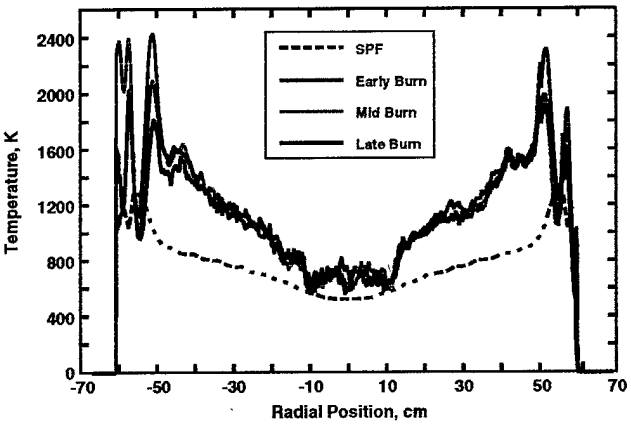

Fig. 9. Measured gas static temperatures of OMS Test.

SSME

An LIF measurement was made on the Space Shuttle Main Engine (SSME) at the NASA Marshall Technology Test Bed (TTB) facility. The purpose of this study was to determine the feasibility of acquiring LIF data for determining flowfield parameters on the SSME. There was great concern as to whether or not the laser systems could maintain optical alignment and single frequency operation during the SSME firings, due to high vibration levels during motor firings. To ensure operation during a motor firing, two complete scanning ring-dye laser systems were set up in the instrument room of the test stand, and the laser beams were routed to the test area via fiber-optic cables. A system layout is shown in Fig. 10. Both laser systems were tuned to the sodium D1 line, 0.5896 microns.

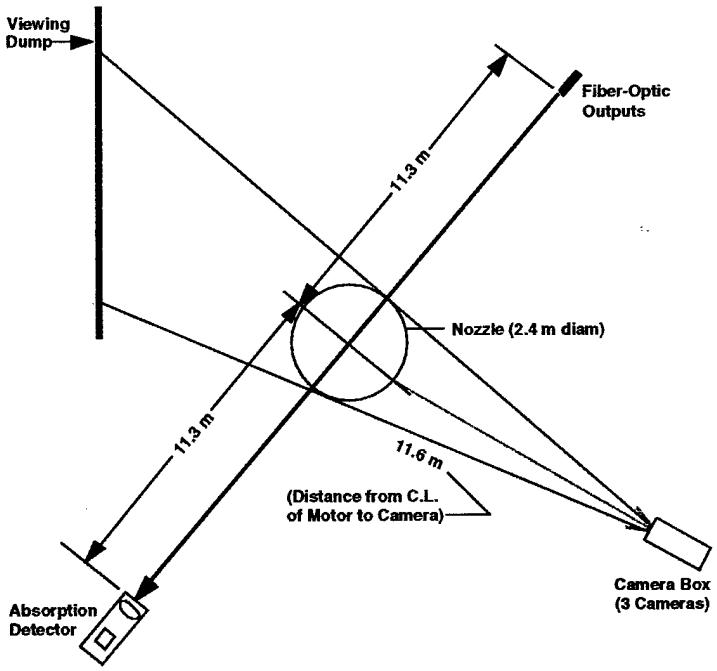

Fig. 10. SSME LIF installation.

The frequency-scanned dye laser outputs were coupled to 33-m optical fibers on the optical bench and routed to the engine deck. Each had a power output of approximately 80 mW. From one laser system, a 1.5-in.-diam collimated beam was generated from the fiber-optic output and directed across the motor centerline approximately 3.5 in. downstream of the nozzle exit plane, while from the second laser system a beam of approximately 2.0 in. in diameter was generated and directed approximately 13.5 in. downstream of the nozzle exit plane. Three cameras viewing perpendicularly to the laser beams were used to view the beams at motor centerline: a Xybion Model 250 intensified CCD camera, an RCA Model TC1030/H24 SIT camera, and a Dage Model CCD 72 CCD camera. All three cameras were equipped with 5-nm optical bandpass filters centered at the D1 sodium line. The Xybion field of view was approximately 122 cm and viewed the motor center line to the edge of the plume; the Dage and RCA cameras were set to provide full-field viewing, or approximately 252 cm. All three cameras were tilted toward the top of the motor to avoid having the Mach disk within the camera viewing area. The output of each camera was recorded on videotape for posttest analysis. Time reference was obtained by recording IRIG time on the videotape.

The laser beam terminated on a photodiode mounted on the opposite side of the test cell to monitor laser beam absorption versus laser frequency. This was to provide a measure of whether or not the plume was optically thin. Laser system specifications are noted in Table 2.

Three SSME firings were conducted during this test program: two 205-sec burns and one 46-sec burn. LIF of the sodium in the engine exhaust was not observed on any of the three firings. This is believed to be due to a combination of collection geometry, low sodium concentration, and insufficient laser beam power densities. It was learned in this technology development program that the laser systems would maintain optical alignment and single frequency operation throughout the full motor firing. This was verified via the system health monitor located in the control room. The laser was somewhat noisy, but the reference fluorescence indicated laser stability was sufficient to tune on and off the absorption line of sodium. All three cameras survived all motor firings, however, the video was saturated during the first motor firing due to sunlight reflection off the test stand structure and the water cooling vapor cloud. To eliminate light scatter off the vapor cloud and structure, a tarp was placed as a viewing dump for the video cameras for the second and third firings. This appeared to provide sufficient blockage of the sunlight and provided a good, dark background for the video cameras. Even with the reduced background on the video cameras, there was no visible fluorescence detected on the final two motor firings. There was sufficient vibration of the fiber-optic output assembly on all firings such that the beam alignment on the absorption detector was lost at motor ignition. Review of the video obtained by the Xybion camera indicates that the laser beam position was still near the nozzle centerline. This was determined by observing particulate scatter of the laser beam from the purge gas through the nozzle after shutdown.

LR91

A simulated-altitude nozzle certification test for a nozzle skirt extension to the LR91-AJ-11 rocket engine using a recently developed Low-Density (LD) quartz phenolic liner was conducted in the J-4 Development Test Cell at AEDC. The test program was conducted using both nozzle skirt extension liner materials, the original asbestos phenolic, and the LD quartz phenolic. Both nozzle liners rely on considerable fuel-film cooling (FFC) for protection. The LR91 is a large, amine-fueled rocket engine used as the second stage of the Titan IV launch vehicle which achieves a thrust level of nominally 105,000 lbf. The basic LR91 engine is constructed with a thrust chamber integrated with a regeneratively cooled nozzle that expands to an area ratio of 12. Inside the chamber, there are 7 axial internal baffles which are cooled by flowing N_2O_4 through them. From there, N_2O_4 sprays into the combustion chamber at the bottom of the baffles. At positions where the baffles are joined to the wall and in the center where the baffles join together, the baffles use fuel cooling rather than oxidizer. A nozzle skirt extension is used in conjunction with the basic chamber-nozzle combination to continue the flow expansion to an exit diameter of 168 cm and an area ratio of 49.2:1. The axial length of the nozzle and skirt extension from the throat to the exit plane is 183 cm. The nozzle and skirt extension liner is film cooled with approximately 16 percent of the total fuel flow being dedicated to film cooling. Note that 12 percent is used for cooling the chamber walls, while the remainder is used for cooling of the baffles. Data from LR91 Tests 3 and 4 tests will be presented for this work.

Since the LR91 test sequence was initially scheduled to have only one firing, it was decided to minimize the risk of data loss by duplicating the measurement. Thus, two complete and independent laser systems which performed redundant tasks were used. These laser systems were installed in an instrumentation building located just outside the test cell. Furthermore, it was desired to traverse the beams across the flow in a plane normal to the plume axis in an attempt to obtain a two-dimensional map of the exhaust flow properties. For Test 3, computer-controlled traversing tables physically translated the fiber-optic head units and the corresponding absorption detectors in a plane normal to the nozzle centerline axis, as shown in Fig. 11a. The motion began at the nozzle centerline, denoted as Station 1, and proceeded in discrete 10-cm steps outward. The relative orientation of the beams with the cameras was maintained at all times, and the beams were traversed to 8 radial stations out to the nozzle boundary (therefore, the last radial station was 70 cm from the nozzle centerline). Prior to engine shutdown, the beams returned to Station 1. For Test 4, the fiber-optic head units remained fixed, and mirrors were mounted to the traversing carts. The beams were traversed through 10 radial stations in 10-cm increments which extended past the nozzle boundary (to a radial station 90 cm from the nozzle centerline), and the beams did not return to Station 1 prior to shutdown. The traverse position was also recorded on the PC data acquisition system for all tests.

Fluorescence detection was done with three unintensified Dage CCD-72 array cameras operating at a standard video rate of 30 frames/sec. Each camera was spectrally filtered with a 10-nm bandpass filter centered about the Na fluorescence line. The large size of the LR91 necessitated the use of 10-nm bandpass filters rather than the 5-nm bandpass filters, due to the increased off-axis rejection of the narrower filters. Camera 1 was set with a 61-cm-diam field of view to provide plume boundary viewing while cameras 2 and 3 had a nominal field of view of 178 cm in diameter to provide full plume diameter viewing, as shown in Fig. 11b. Cameras 1 and 2 utilized computer-controlled zoom lenses to optimize the spatial resolution at each traverse position

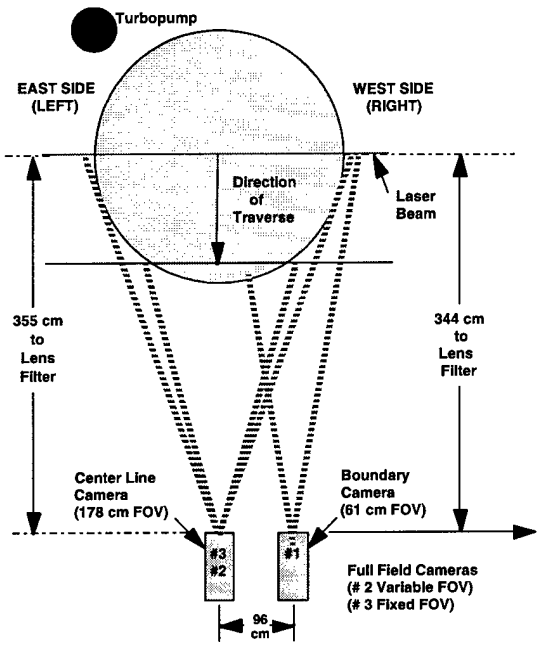

a. Top view

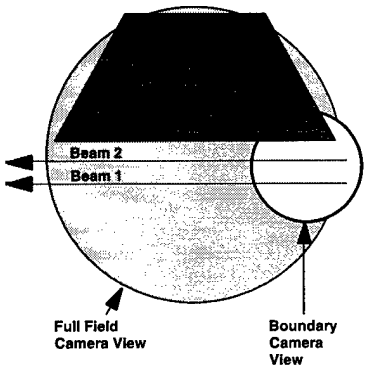

b. Side view

Fig. 11. LIF installation for LR91 testing.

of the laser beams. Measurements of transmission versus radial position were made on each camera/filter assembly for each lens setting in order to account for the angular dependence of the overall video response. The video signals from cameras 1 and 2 were sent to the main control room where they were recorded onto two independent Sony D-2 digital recorders. Additionally, the video signals from each camera were fed into the laser area where they were recorded onto three independent Panasonic VHS recorders as a backup. The beam from laser system #2 was located 7.62 cm axially downstream of the nozzle exit, while the beam from laser system #1 was located axially 15.24 cm downstream of the nozzle exit. In Test 3, the two beams propagated in opposite directions, while in Test 4, they both propagated from the same side.

For the LR91, considerable background illumination was present, due in part to test cell lighting for other diagnostic measurements. The 10-nm filters, as opposed to the 5-nm filters used for OMS, gave a higher level of plume visible radiance than the OMS, and numerous objects with highly reflective surfaces near the test article. Hence, significant portions of some of the LR91 LIF signal profiles were fatally corrupted by the background.

The LR91 test results are greatly influenced by the fact that the nozzle cooling mechanism is a reliance upon heavy amounts of fuel-film cooling (FFC). Since Na is a trace species of the fuel, the heavy FFC led to very significant Na densities in the boundary layer of the exhaust flow. In fact, a review of the data establishes that the plume structure can be categorized into three distinct annular regions. The outermost region was thin, ~ 1 cm, and contained a Na density that led to reasonable fluorescence measurements. Inward of the thin sheath was a~10-cm region of very high Na density, as well as particulates, which was directly attributable to the nozzle FFC. The remaining core of the exhaust flow could again be characterized as having suitable Na densities for fluorescence measurements. While the outer sheath region and the inner core flow were anticipated prior to testing, the existence of a physically and optically thick layer composed of particulates and very high Na concentration was unexpected. In the FFC region the particulate component of the video signal presented a minor inconvenience for the LIF analysis by decreasing the effective dynamic range and producing a nonzero baseline in certain portions of the flow. However, the more important factor in the LIF analysis is the extreme optical depth of the FFC layer. In fact, it was found that at the Na line center frequency, the laser beam was totally absorbed. However, the laser beam did propagate through the FFC layer at frequencies off line center, and fluorescence was observed in both the particle layer and the inner core flow.

The video data acquired by Camera 1 from Test 3 at the 7.62-cm downstream position, i.e., laser 2, near the flow radial periphery displayed considerable Na fluorescence. As mentioned above, the data reduction process generates a spectral line at each point in the flow along the laser beam. The map given in Fig. 12 displays the Na fluorescence data of Camera 1 as was done in Fig. 5, with the frequency in the vertical dimension corresponding to−18 GHz and +12 GHz at the upper and lower edges, respectively, relative to the Na fluorescence line of the reference cell. The horizontal dimension is the field of view of Camera 1, corresponding to an absolute radial position in the flow from 58 to 98 cm relative to the nozzle centerline axis. The outermost plume fluorescence begins at~ 94 cm. For radial positions between 90 and 88 cm in Fig. 12, the camera was saturated, and information on the peak intensity was lost. However, this represented no significant loss of information since the spectral fitting utilized the line wings. The centroid of the fluorescence displays a monotonic trend to more positive frequencies from 94 cm all the way to~ 85 cm, at which point the velocity reaches a maximum. At positions interior 85 cm of Fig. 12, a given fluorescence line, i.e., a vertical or frequency profile, appears to have two peaks. This is simply due to the strong laser beam attenuation of the frequency-shifted line center by the optically dense outer portion of the flow. Yet there is considerable fluorescence in the wing of the Na line, indicating a

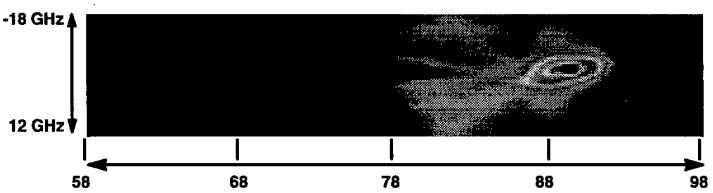

Fig. 12. Fluorescence signal acquired during one laser scan from LR91 Test 3.

high Na density. Inward of 78 cm, there is a precipitous drop in the Na density, indicating the boundary between the inner core flow and the particulate region discussed above. There is weak fluorescence in this region, although the S/N ratio is very small.

Vertical profiles of Fig. 12 were taken, analogous to those shown in Fig. 7. It was found that in the very narrow region outside the FFC layer, the Na fluorescence displayed the usual hyperfine structure. However, as one moves further into the FFC layer, the optical depth significantly attenuates the line profile, precluding a simple determination of the gas static temperature in the FFC region. Spectra acquired within 78 cm, in the low Na density core flow, suffered from a low signal-to-noise ratio. This is largely due to the fact that only the far wings of the lines were obtainable, since the kernel of the line was absorbed in the FFC region.

Although the temperature was indeterminable in this flow, the radial velocity is rather insensitive to homogeneous line profile distortions. Hence, the spectral lines, using either the complete profile or only the wings, were fit and a comparison was made to the SPF results. These are shown in Fig. 13 for Test 3. The agreement of the data with the prediction of the location and value of the radial velocity of the plume shear layer at the 7.62 cm axial position is quite satisfactory. It is interesting to note, though, that the data indicate a slightly wider shear layer than the predictions. The systematic uncertainty of the radial velocity was estimated to be$\pm 10^4$ cm/sec for a laser frequency scan period of slightly less than 5 sec.

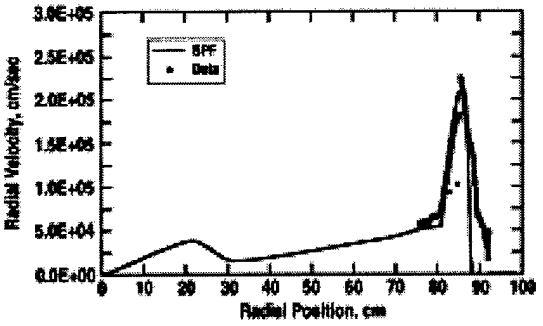

Fig. 13. Comparison of the measured radial velocity with the SPF predictions, Test 3.

The LIF data from Test 4 were manipulated in a similar manner to that of Test 3. However, in this case, Laser 1 (at the 15.24 cm axial position) was utilized. The character of Test 4 data is similar to that of Test 3, and only the final results are given here for brevity. A plot of the fit results for the radial velocity is given in Fig. 14. The results compare favorably with the SPF predictions at 15.24 cm downstream of the nozzle exit. Curiously, the data seem to indicate a thinner shear layer than that predicted by SPF. As before, the optical depth of the FFC region was excessive in Test 4, and no accurate temperature information can be derived from this data.

A fortunate turn of events during this test was the combined use of the laser attenuation and scattering data to ascertain the identity of the particles in the flow. After considerable analysis, it was discerned that the particles were unvaporized AZ50 droplets which survived the combustion process due to the significant amount of FFC used in this motor and nozzle assembly.

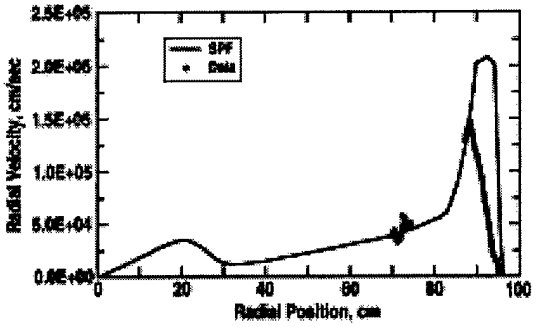

Fig. 14. Comparison of the measured radial velocity with the SPF predictions, Test 4.

CONCLUSIONS

Overall, the Na LIF measurements performed on vastly different full-scale rocket engines at both sea-level and simulated altitude conditions were highly successful. The initial work on the DTF demonstrateed the potential that Na LIF probing of rocket flows has in providing crucial information on nozzle design, thermal integrity, and combustor mixing and performance.

The OMS program provided an excellent data set which yielded gas static temperature, radial velocity, and fuel distribution. Part of this success is due to a very low background light level, resulting in very clean data signals. The agreement of SPF modeling of the shear layer with the data was encouraging, but points out areas for code improvement. Furthermore, the SPF modeling of the centerline flow needs review for the case of the OMS engine. The data show a much more dynamic region, with the flow reversing radial direction twice near the core, and with significant magnitudes which were much greater than predicted. The temporal effect of the OMS flow-field boundary is interesting in that it may shed light on the heat-transfer characteristics of the nozzle itself, while it was seen that the static temperature of the inner core flow was extremely steady during the burn duration.

The SSME effort indicated the difficulty in attempting to probe an extremely large motor in daylight. Presumably, the fluorescence levels fell below the background levels and could not be distinguished. Hence, future diagnostics of the SSME should consider other schemes such as night testing or very narrow line filters with the associated narrow angular field of view.

The results of the LR91 work indicated the robustness of the radial velocity measurement, even in the face of an extremely optically thick environment. Future work with such very heavily fuel-film cooled motors should take into consideration the severe distortion of the fluorescence spectral line profile boundary layer when attempting temperature determination, even though the velocity determination is oblivious to this effect. An important LR91 result is the observance of the AZ50 droplets in the flow. While this result was not anticipated, the data are consistent with this identification for the particles. It would be useful to carry out a dedicated test sequence which defines the minimum FFC level to operate the LR91, or other FFC engine, in order to maximize payload capabilities.

A desired improvement for future measurements is the reduction of the background signal, in order to raise the LIF signal-to-noise ratio. In the LR91, the tradeoff to obtain the entire nozzle coverage at the expense of a narrow bandpass filter was too much in favor of the spatial coverage. In future efforts, a reduced field of view should be accepted, if need be, in favor of the narrow filters. For heavily fuel-film cooled rocket engines, the problem of optical depth remains, without a simple resolution. A possible alternative, which still exploits Na in the fuel, is to incorporate a pump-probe arrangement. Regardless, pretest efforts to quantify the amount of Na present in the fuel should be increased.

In addition, the next phase of development of this technique is further reduction of complexity and the associated costs in an attempt to make Na-based LIF a practical diagnostic tool for routine use. This currently involves automating the laser and camera control systems and reducing the data reduction procedure.

REFERENCES

1. Brasier, C. W., Drakes, J. A., Anspach, K. M., Porter, R. G., Simmons, M. A., and Pruitt, D. W., "Laser-Induced Fluorescence Measurements of OMS and LR91 Amine Rocket Exhausts," AIAA Paper No. 97-2378, Atlanta, GA, June 1997.

2. Aerojet-General Corporate Report No. LRP198, "Storable Liquid Propellants, Nitrogen Tetroxide/Aerozine 50," June 1962.

3. Schmidt, E. W., *Hydrazine and Its Derivatives* John Wiley & Sons, NY, 1984.

4. Fairbank, W. M., Hansch, T. W., and Schalow, A. L.,*J. Opt. Soc. Am.*, Vol. 65, 1975.

5. Brasier, C. W. and Porter, R. G., "Development of a Laser-Induced Fluorescence System for Application to Rocket Plumes," AEDC-TR-92-6 (AD-A259760), January 1993.

6. Press, W. H., Flannery, B. P., Teukolsky, S. A., and Vetterling, W. T., *Numerical Recipes*, Cambridge University Press, 1986.

7. Cheng, S. S., "Resonant Doppler Velocimetry in Supersonic Nitrogen Flow," Ph.D. Dissertation, Princeton University,1982.

8. Nickerson, G. R., "Two-Dimensional Kinetics (TDK) Nozzle Performance Computer Program," NASA-36863, March 1989.

9. Wolf, D. E., Dash, S. M., and Pergament, H. S., "A Shock-Capturing Model for Two-Phase Chemically Reacting Flow in Rocket Nozzles," AIAA Paper No. 85-0306, Reno, NV, January 1985.

REPORT DOCUMENTATION PAGE

Form Approved
OMB No. 0704-0188

1. AGENCY USE ONLY *(Leave blank)*	2. REPORT DATE	3. REPORT TYPE AND DATES COVERED
	Oct 12 - 24, 1997	Technical Society Paper

4. TITLE AND SUBTITLE
Application of Laer-Induced Fluorescence (LIF) to Liquid-Propellant Rocket Engine Testing

5. FUNDING NUMBERS
Job No. 0094

6. AUTHOR(S)
Brasier, C. W., Drakes, J. A., and Simmons, M. A.

7. PERFORMING ORGANIZATION NAME(S) AND ADDRESS(ES)
Sverdrup Technology, Inc., AEDC Group
Arnold Engineering Development Center
Arnold AFB, TN 37389-9011

8. PERFORMING ORGANIZATION REPORT NUMBER

9. SPONSORING/MONITORING AGENCY NAME(S) AND ADDRESS(ES)
Arnold Engineering Development Center
Air Force Materiel Command
Arnold AFB, TN 37389-9011

10. SPONSORING/MONITORING AGENCY REPORT NUMBER

11. SUPPLEMENTARY NOTES
Also available as inclusion in proceedings of 90th Propulsion & Energetics Panel (PEP) AGARD conference in Brussels, Belgium on October 20-24, 1997.

12a. DISTRIBUTION AVAILABILITY STATEMENT
Approved for public release; distribution unlimited.

12b. DISTRIBUTION CODE
A

13. ABSTRACT *(Maximum 200 words)*

Combustion exhausts present a challenging problem for researchers due to the extremely harsh environment, and non-intrusive diagnostics are often sought to provide flow property information. Laser-induced fluorescence (LIF) is one technique in which a chosen flow molecule or marker is probed to yield gross flow properties, such as static temperature and flow velocities. The work presented herein describes the application of LIF to the combustion exhausts of several full-scale liquid-propellant rocket engines spanning a wide range of operational parameters. The method is based upon the use of cw ring-dye lasers which scan in frequency over either the Na D 1 or D 2 line at 5896 and 5890 Ĺ. Na is used as a basis for this approach since it occurs as a trace element in both hydrogen and amine rocket fuels. The generic apparatus is described, including a discussion of the collection and interpretation of the LIF signal to yield radial and temporal profiles of radial flow velocity, static temperature, and fuel distribution. It was found that the LIF technique provides quality data in most cases. Certain stressing situations were also found in which data on the flow properties were not obtainable. Also, computational fluid dyanamics (CFD) modeling of the plumes was used to provide baseline estimates of the exhaust flow properties. The model reasonably predicted the gross behavior of the flow as determined by the LIF technique, although some items of fine spatial structure were not reproduced very well.

14. SUBJECT TERMS	15. NUMBER OF PAGES
laser-induced fluorescence, rocket plumes	11
	16. PRICE CODE

17. SECURITY CLASSIFICATION OF REPORT	18. SECURITY CLASSIFICATION OF THIS PAGE	19. SECURITY CLASSIFICATION OF ABSTRACT	20. LIMITATION OF ABSTRACT
Unclassified	Unclassifeid	Unclassified	UL